

## Article

# Investigation of Indoor Asymmetric Thermal Radiation in Tibet Plateau: Case Study of a Typical Office Building

Meilin Wang  and Pengyuan Shen \* 

School of Architecture, Harbin Institute of Technology, Shenzhen 518055, China; wangmeilin1107@163.com

\* Correspondence: pengyuan\_pub@163.com; Tel.: +86-137-6460-266

**Abstract:** The unique climate in cold plateaus leads to long and cold winters, which result in the characteristics and creation of an indoor thermal environment different from that of plain areas. However, there is a lack of detailed research on and evaluation of indoor temperature distributions. This study took an office building in Lhasa as an example to study the indoor non-uniform temperature distributions with radiator and solar radiation. The indoor and outdoor thermal environment parameters were tested. Next, a numerical model was established and verified. On a typical winter weather day, although the average indoor air temperature and radiation temperature in Lhasa are higher than those in Beijing (both are cold areas), the temperature in both is lower than comfortable levels. The indoor vertical air temperature differences are below 3 °C, with a 5% dissatisfaction most of the time. Solar radiation and radiators seriously affect the uniformity of the indoor thermal environment. The radiation asymmetry in Lhasa is significant, and the maximum radiation temperature asymmetry can reach 8.73 °C. In addition, the setting of north-facing windows should be avoided as far as possible in Tibetan areas. Suitable design and evaluation standards should pay attention to the obvious phenomenon of uneven indoor temperature distribution.

**Keywords:** Tibet Plateau; field test; vertical temperature difference; radiant temperature asymmetry; numerical simulation



**Citation:** Wang, M.; Shen, P. Investigation of Indoor Asymmetric Thermal Radiation in Tibet Plateau: Case Study of a Typical Office Building. *Buildings* **2022**, *12*, 129. <https://doi.org/10.3390/buildings12020129>

Academic Editors: Bo Hong, Yang Geng and Dayi Lai

Received: 28 December 2021

Accepted: 24 January 2022

Published: 26 January 2022

**Publisher's Note:** MDPI stays neutral with regard to jurisdictional claims in published maps and institutional affiliations.



**Copyright:** © 2022 by the authors. Licensee MDPI, Basel, Switzerland. This article is an open access article distributed under the terms and conditions of the Creative Commons Attribution (CC BY) license (<https://creativecommons.org/licenses/by/4.0/>).

## 1. Introduction

Tibet is called the “Roof of the World” and the “Third Pole of the Earth” [1] due to its average altitude of over 4000 m and unique ecological features [2]. There is a population of approximately 3.44 million currently residing in Tibet [3]. The climate in the Tibetan Plateau has several peculiar characteristics, such as low atmospheric pressure, low atmospheric humidity, small seasonal temperature fluctuation and wide diurnal temperature range, and strong solar radiation [1]. Compared with plain areas, the annual average temperature in Lhasa and Xigaze is 10 °C–15 °C lower than that in Chongqing, Wuhan, and Shanghai at similar latitudes, but the solar radiation in Lhasa is a third higher than in those cities, and sometimes even twice as high [1]. The indoor thermal environment of the Tibetan Plateau is more susceptible to the outdoor climate, making it more difficult to create a comfortable indoor thermal environment, especially during its long and cold winters.

The mean indoor air temperature of the Tibet Plateau in winter is very low, only 5–12 °C for rural buildings [4] and 3.8–7.8 °C for traditional houses [5] in Lhasa; 2.8 °C in Kangding [6]; 4.16 °C in Nyingchi [7]; 2.5 °C in Gannan [8]; and 6 °C in Qamdo [9]. The indoor air temperature can reach 15 °C with space heating [10] or 11.5 °C with passive solar design [11]. However, the range of operating temperature during winter in Lhasa varies from 12.74 °C to 23.15 °C [10,12,13], and the acceptable temperature range is 13.16 °C–26.76 °C [9]. The thermal discomfort rates are 66% [11] and 68% [13]. Based on the existing research results, residents feel dry [11,12], and the resulting discomfort rate ranges from 10% to 57.4% [4,7,9,12,14]. However, some researchers found that the indoor thermal environment satisfaction rate is 90% and the low humidity does not have negative

impacts [15]. Moreover, the perception of discomfort can also be attributed to the special characteristics of solar radiation, sky background temperature, and outdoor temperature in Tibet, which makes the internal surface temperature vary greatly between walls and leads to variations in radiative heat exchange differences between the human body and each internal surface. Hence, asymmetric radiation is an obstacle to achieving satisfying indoor thermal comfort in Tibet.

Fanger proposed the concept of “radiant temperature asymmetry (RTA)” based on a series of thermal sensation experiments; the concept is defined as the difference between the radiation temperature of the plane of the two opposite sides for a small plane element or of the environment on opposite sides of a person, and is evaluated by the percentage of dissatisfaction [16,17]. In winter, RTA in a space may be caused by cold windows, walls, floors, ceilings, and heating panels on the wall, ceiling, and floor. Some studies involved the investigation of the effects of vertical radiant asymmetry. However, their conclusions differ. Chrenko [18] found that the comfort limit for vertical RTA caused by heated ceilings was 2 °C. The work conducted by Fanger et al. [17] has shown that the vertical RTA of 14 °C for cool ceilings and 4 °C for the warm ceilings could be tolerated without adversely affecting comfort, but the results of Loveday and Hodder et al. [19,20] and Griffiths and McIntyre [21] have shown that there is no effect of vertical radiant asymmetry from cool (warm) ceilings on thermal comfort. Furthermore, the comfort limits for horizontal radiant asymmetries from walls (windows) are different. In the study by McNall and Biddison [22], the occupants felt uncomfortable when the temperature of the warm wall reached 35 °C higher than ambient temperature, and the temperature difference between cool walls and other walls was more than 11.1 °C. In addition, Fanger [17] recommended that the radiant temperature asymmetries between warm walls and the cool walls should be 23 °C and 10 °C, respectively. Hence, although RTA is an accepted and promoted metric in the thermal comfort evaluation, there are remaining research questions concerning consensus on comfort bounds and systematic understanding in various indoor environmental settings, such as RTA caused by windows and radiators, among others.

The International Standards Organization (ISO) 7730-2005 [23] and the American Society of Heating, Refrigerating and Air-Conditioning Engineers (ASHRAE) standard 55-2017 [24] prescribe limits for radiant asymmetry, but the limits are different based on different conditions. The ISO 7730-2005 standard prescribes the limit value of RTA caused by warm ceilings, cool walls, cool ceilings, and warm walls, and the percentage of those dissatisfied as a function of the RTA are 5% (category A and B) and 10% (category C) [23]. However, to better control local discomfort, when a seated occupant wears standard clothing and is exposed to comfortable operative temperature and not in a draught, ASHRAE recommends that the RTA should be less than 5–23 °C by testing the radiation temperatures on opposite planes of a small plane element with a height of 0.6 m (the height at the ‘center’ for a seated person) [24]. The comfort limits of the RTA were only applicable to specific geometries and conditions in the experiment. In practice, the angle factors in the cold or warm part of the panel are diverse, and the parameters of the indoor thermal environment are changeable and asymmetrical. Moreover, the RTA of the three-dimensional human body is different from that measured with a planar element, especially in a confined space. As a consequence, defining comfort limits for RTA is not easy work.

However, there is a lack of relevant studies on the phenomenon of non-uniform indoor temperature distribution and its evaluation in the Tibetan Plateau. The temperature differences of windows, wall, floors, and ceilings can be severe in this area. Especially when radiators are used for space heating, the temperature difference between panels can be further exacerbated. Thus, the influence of asymmetrical temperatures on the thermal environment cannot be ignored. Furthermore, when the radiator is working, the occupiers can potentially suffer from radiant asymmetry due to the cold panels (windows, floor, and walls) and warm panels (windows and radiators) at the same time. In addition, the temperature of windows may vary greatly between the morning and the afternoon, during which cold panels may become warm due to the strong solar radiation. However, these

unique situations have not been considered in other studies. Therefore, a field test and numerical simulations were carried out in a typical office building in Lhasa to analyze the non-uniform distribution of the thermal environment. Moreover, the indoor thermal characteristics on a typical-weather day in the plateau (Lhasa) and plain (Beijing) cities in cold regions [25] were compared and analyzed. The degrees of VATD and RTA were quantitatively assessed as well as the corresponding percentage of dissatisfaction. This research will help to better understand, design, build, and evaluate indoor thermal comfort in the Tibetan Plateau.

## 2. Methodology

In this study, the indoor and outdoor environmental parameters of an office building were collected through on-site measurement, and the CFD simulation results were verified by the measured parameters. Both experimental data and simulation results were used for indoor temperature distribution analysis. In addition, to further study the uniqueness of the indoor thermal environment in the Tibet Plateau in the typical weather day of winter, the same computational model was used and the simulation results of Lhasa and Beijing were analyzed comparatively. At the same time, taking into account human exposure positions when the vertical air temperature difference (VATD) and RTA were evaluated. Figure 1 shows the framework of this study.

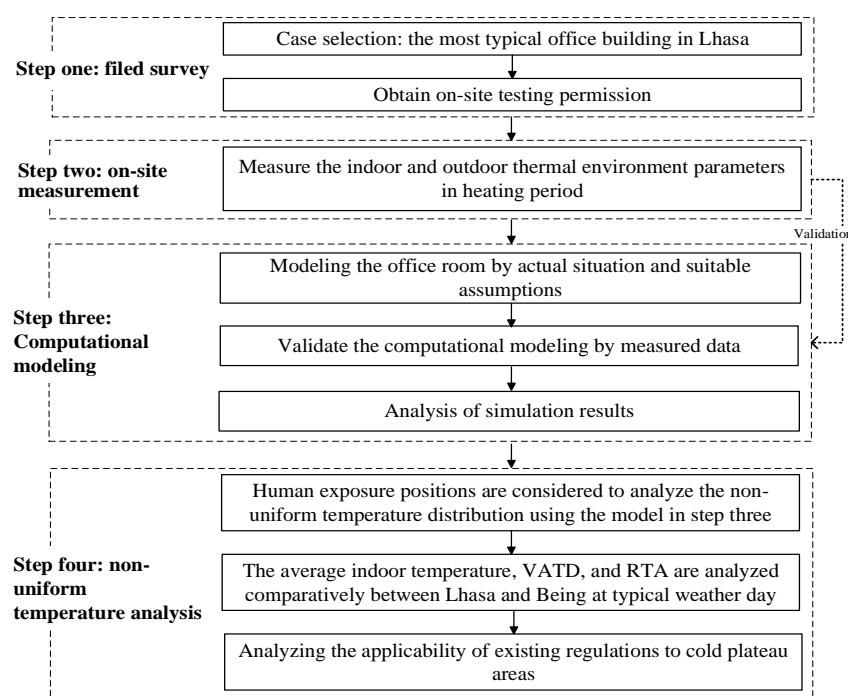


**Figure 1.** Research flow chart.

### 2.1. Field Test

Lhasa is located in the southeastern part of the Tibetan Plateau, with an altitude of 3648.9 m. The geographical coordinates are  $91^{\circ}06'$  east longitude and  $29^{\circ}36'$  north latitude. According to the “Building Climatic Zone Classification Standard” (GB 50178-93) [25] and the “Design Code for Heating Ventilation and Air Conditioning of Civil Buildings” (GB 50736-2012) [26], Lhasa is a cold area and a heating area. A typical office building was selected in Lhasa (see Figure 2) for this research. Due to the abundant solar energy, the window-to-wall ratio of the south wall reached 0.53; detailed information is shown in Table 1. The height difference between the indoor and outdoor areas is 750 mm, the total building area is 1821.32 m<sup>2</sup>, and the story height is 3 m. Furthermore, this is a mixed-structure building. The wall adopts a concrete solid block 240 mm thick; the thermal

properties of the enclosure structures is shown in Table 2. The windows use double-tempered insulating glass with a 9 mm air layer. As shown in Figure 3, all the offices are heated by radiators, which are installed under the south windows.

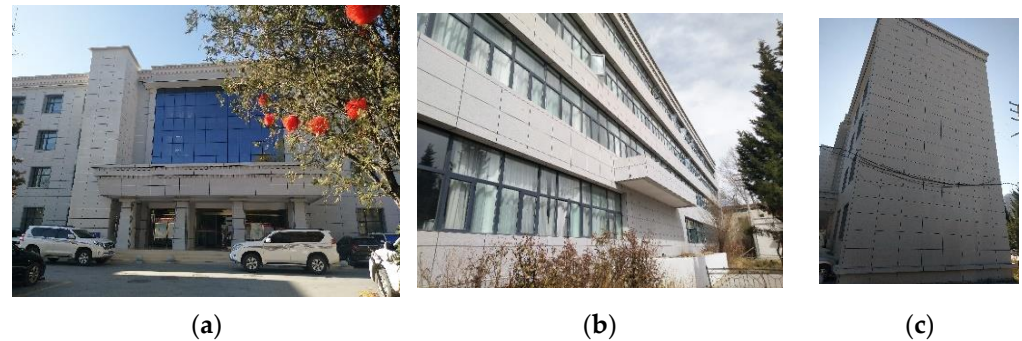


**Figure 2.** The selected typical office building in Lhasa: (a) north facade; (b) south facade; (c) west faced.

**Table 1.** The window-to-wall ratio of the office building.

Direction	Area of External Window (m <sup>2</sup> )	Area of the External Wall (m <sup>2</sup> )	The Ratio of Window to Wall
East	43.2	162.00	0.27
South	360	673.20	0.53
West	0	162.00	0
North	201.3	673.20	0.3

**Table 2.** Thermal properties of the building structure.

Type	Heat Transfer Coefficient (W/m <sup>2</sup> ·K)	Thickness (mm)
External wall	0.54	316
Roof	0.412	280
Floor	1.65	420
Partition	1.55	310
External window	3.2	5 (glass) + 9 (air) + 5 (glass)

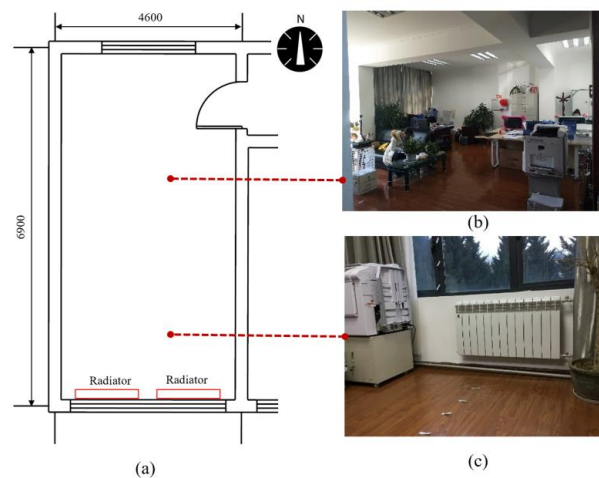


**Figure 3.** The office room of the building selected: (a) the general layout of the office room; (b) the state of the office room; (c) the south windows and radiator.

The field experiments were carried out from 14 to 16 March in 2018. The measured environmental parameters include indoor and outdoor air temperature, humidity, and wall

temperature. The following devices were used to measure the variables: a HOBO U12-012 digital temperature and humidity meter and a Testo 830-T4 handheld infrared thermometer. Those can be seen in Figure 4. The specifics of each device are given below:

1. HOBO U12-012 digital temperature and humidity meter:



**Figure 4.** Experimental instruments: (a) HOBO U12-012; (b) Testo 830-T4.

Temperature range:  $-20$  to  $70$  °C; accuracy:  $\pm 0.21$  °C; humidity range: 1–95%; accuracy:  $\pm 2.5\%$ .

2. Testo 830-T4 handheld infrared thermometer:

Temperature range:  $-30$  to  $350$  °C; accuracy:  $\pm 2\%$ .

The field measurements were carried out based on the method recommended in ASHRAE 55-2017 [27]. More specifically, for the outdoor environmental parameters, the location of the measuring points was open ground near the office building at a height of 1.1 m without direct sunlight. For the indoor environmental parameters, a measuring point at a height of 1.1 m in an occupied office room was selected as the representative point for the measurement of air temperature and relative humidity because the occupants were usually in a sitting position in the office. The measuring points for internal wall temperature were located on the central line of the east and west wall, and the points of the north wall are 30 cm away from the west wall with the height of 50 cm, 75 cm, 100 cm, 125 cm, 150 cm, 175 cm, 200 cm.

## 2.2. Simulation and Assumptions

### 2.2.1. Governing Equations

Since there is no ventilation equipment and the door and windows are closed during working hours, the office can be regarded as a closed cavity. Thus, when the indoor natural convection heat transfer was calculated, the Boussinesq approximation for thermal buoyancy was used to deal with the buoyancy term caused by the temperature difference [28]. The Boussinesq approximation hypothesis consists of neglected viscous dissipation in fluids, constant physical properties, and fixed density (density variations are considered only for terms related to momentum equation and volume force). The fluid was in compressible flows in a steady-state so that the air density  $\rho$  in the gravity terms can be expressed as [28]:

$$\rho = \rho_c [1 - \alpha(T - T_c)] \quad (1)$$

where  $\rho_c$  is air density at corresponding  $T_c$ ,  $\text{kg}/\text{m}^3$ ;  $\alpha$  is the coefficient of cubical expansion; and  $T$  and  $T_c$  are the air temperature and reference air temperature, °C.

Reynolds-averaged Navier–Stokes (RANS) was used to model the conservation of momentum energy and mass. Based on the Boussinesq vortex viscosity hypothesis, the basic equations applicable to natural convection heat transfer problems are as follows [29]:

$$\frac{\partial u_i}{\partial x_i} = 0 \quad (2)$$

where the  $u_i$  is the air velocity component in point  $x_i$ , m/s and  $x_i$  is the distance of the point  $x_i$  for origin, m.

$$\frac{\partial \rho u_i u_j}{\partial x_j} = -\frac{\partial P}{\partial x_i} + \frac{\partial}{\partial x_j} \left[ (\mu + \mu_t) \left( \frac{\partial u_i}{\partial x_j} + \frac{\partial u_j}{\partial x_i} \right) \right] + \rho_c \beta g_i (T - T_C) \quad (3)$$

where  $u_j$  is the air velocity component in point  $x_j$ , m/s;  $P$  is the partial pressure of water vapor in moist air, Pa;  $\mu$  is dynamic viscosity, (N·s)/m<sup>2</sup>;  $\mu_t$  is turbulent viscosity, (N·s)/m<sup>2</sup>;  $g_i$  is the gravitational acceleration vector, m/s<sup>2</sup>; and  $\beta$  is the thermal expansion coefficient, K<sup>-1</sup>.

The energy equation is as follows [30]:

$$\rho C_p V \cdot \nabla T = \lambda_{eff} \nabla^2 T \quad (4)$$

where  $C_p$  is the specific heat of the air, J/(kg·K) and  $\lambda_{eff}$  is the effective thermal conductivity (W/m·°C), which can be represented as:

$$\lambda_{eff} = \frac{C_p \mu_t}{Pr_t} + \lambda_l \quad (5)$$

where  $Pr_t$  is turbulent Prandtl number and  $\lambda_l$  is the laminar effective thermal conductivity, W/m·°C.

### 2.2.2. Solution Methods

According to the computational model and theoretical analysis, the indoor airflow pattern of the office room is generally of natural convection. The Rayleigh number is usually used as a criterion to distinguish laminar flow from turbulent flow [31]. The numerical simulation method is based on the Rayleigh-averaged equation, and the indoor zero-equation model is chosen for this model. The turbulent viscosity  $\mu_t$  is expressed by Equation (6) [32].

$$\mu_t = 0.03874 \rho v l \quad (6)$$

where  $v$  is the local mean velocity, m/s and  $l$  is the nearest distance from the wall, m.

Moreover, the indoor airflow has turbulence characteristics, while the floor, window, and walls are the starting areas of the turbulent flow, which is a laminar or quasi-laminar zone. Hence, the high-Reynolds-number turbulence model is not applicable. Unlike the solution of the high-Reynolds-number turbulence model, the wall function model combines the physical quantity of the wall and the variables of the turbulence development zone in this computational model. The non-dimensional parameters  $u^+$  and  $y^+$  can give an accurate description of the issue, which can be calculated by:

$$u^+ = \frac{u}{u_\tau} \quad (7)$$

$$y^+ = \frac{\rho_w u_\tau y}{\mu_l} \quad (8)$$

where  $u$  is the tangential velocity of the wall, m/s;  $u_\tau$  is the friction velocity of the wall, m/s;  $\rho_w$  is the density of the wall, kg/m<sup>3</sup>; and  $y$  is the normal distance from the wall to the first layer of mesh, m. The results show that the  $y^+$  was within the range of 30 to 150.

In this study, air does not participate in the radiation heat transfer in space, and the surfaces are assumed to be diffused. In addition, the radiation model is used to study the radiation heat transfer of the enclosure structure, the radiator, and the human body when the occupier is in different positions. The discrete ordinate radiation model is as follows [33]:

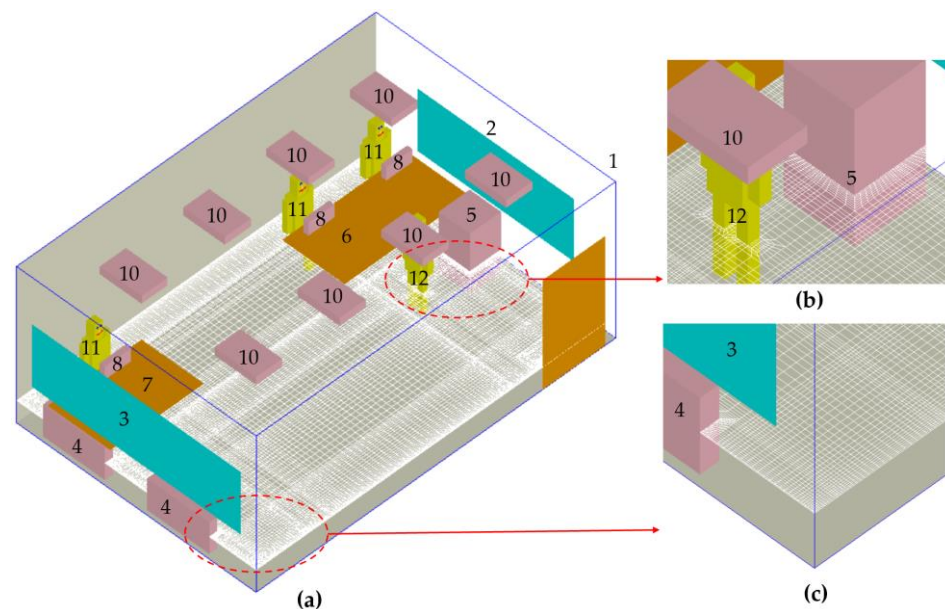
$$\nabla \cdot \left( I(\vec{r}, \vec{s}) \vec{s} \right) + (a + \sigma_s) I(\vec{r}, \vec{s}) = an^2 \frac{\sigma T^4}{\pi} \int_0^{4\pi} I(\vec{r}, \vec{s}') \Phi(\vec{s}, \vec{s}') d\Omega' \quad (9)$$

where the  $\vec{r}$  is position vector;  $\vec{s}$  is a directional vector;  $\vec{s}'$  is scattered direction;  $s$  is the length path, m;  $a$  is absorption coefficient;  $n$  is convert coefficient;  $\sigma_s$  is scattering coefficient;  $\sigma$  is the Stefan–Boltzmann constant,  $5.672 \times 10^{-8} \text{ W/m}^2\text{K}^4$ ;  $I$  is radiation intensity depending on location ( $\vec{r}$ ) and direction ( $\vec{s}$ ),  $\text{W/m}^2$ ;  $\Phi$  is phase function; and  $\Omega'$  is the spatial angle.

The solver of the CFD model used the finite volume method, because it constructs discrete equations from a physical standpoint, while each discrete equation defines the conservation of a physical variable for a finite volume. Hence, the equations are always conservative. In addition, the SIMPLE algorithm that is sequentially close to the approximate solutions of linear algebraic equations is used.

### 2.2.3. Computational Modeling

To investigate the indoor thermal environment characteristics in Lhasa, a 3 dimensional computational office model was built based on the real scenario. The geometry and surface mesh are shown in Figure 5, and the model was constructed and computed in Fluent Airpak 3.0.16. The computational model consists of walls, windows, seated persons, standing persons, lights, etc., and the detailed parameters of each item are shown in Table 3. The default person modules were used as the standing and sitting person models in this study. The numbers in Table 3 correspond to Figure 5. In addition, the computers were hidden under the desks.

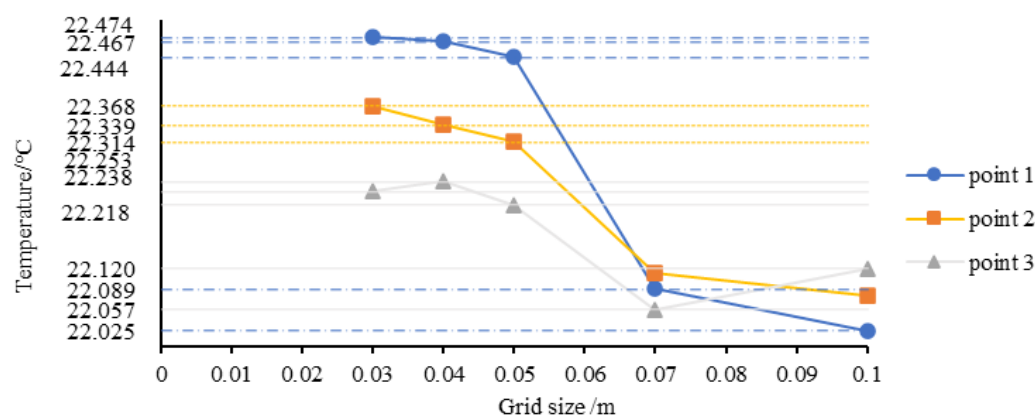


**Figure 5.** The 3D model and detailed mesh: (a) computational model; (b,c) drawing of partial enlargement.

**Table 3.** The parameters of the computational model of the office.

Number	Type	Size	Amount	Heat/Temperature
1	Office	4.6 m × 6.9 × 3 m	1	—
2	South-facing window	3.6 m × 1.2 m	1	—
3	North-facing window	1.8 m × 1.2 m	1	—
4	Radiator	1.2 m × 0.15 m × 0.6 m	2	51.5 °C [34]
5	Printer	0.6 m × 0.65 m × 1.15 m	1	80 W
6	Desk 1	2.4 m × 1.2 m × 0.75 m	1	—
7	Desk 2	1.8 m × 1.2 m × 0.75 m	1	—
8	Screen	0.5 m × 0.1 m × 0.25 m	4	40 W
9	Computer	0.15 m × 0.28 m × 0.35 m	4	120 W
10	Lamp	0.5 m × 0.8 m × 0.15 m	8	34 W
11	seated person	0.4 m × 0.35 m × 1.1 m	3	69.78 W [35]
12	Standing person	0.3 m × 0.2 m × 1.7 m	1	93.04 W [35]

In order to determine the suitable meshing scheme, the grid independence tests were carried out by different numbers of elements. Five grid sizes were considered: 0.1 m, 0.07 m, 0.05 m, 0.04 m, and 0.03 m. Furthermore, the temperatures of points (1.95, 1.1, 3), (1.95, 1.1, 3.45) and (1.95, 1.1, 3.9) are connected in Figure 6. The temperature of the three points changes little when the grid decreases from 0.05 m to 0.03 m. This shows that the impact of grid size on the simulation results can be ignored when the grid size is equal to or smaller than 0.05 m. The results showed that the computational domain was divided into 279,146 small hexahedron cells with finite volumes under optimal grid size. An acceptable grid quality was obtained in which the elements less than 0.15 were severely distorted (Figure 6). The convergence criteria were the solutions of nonlinear equations and relative errors with tolerances from  $1 \times 10^{-7}$  to  $1 \times 10^{-3}$ . The residuals of momentum were below  $1 \times 10^{-3}$ . The simulation converged in 1123 iterations.

**Figure 6.** Grid independence verification results.

#### 2.2.4. Operating Environment and Boundary Conditions

Lhasa is 3650 m above sea level. The atmospheric pressure and air density are 64.504 kpa and  $0.764 \text{ kg/m}^3$ , respectively. In addition, when setting the solar radiation, geographic coordinates of  $91^{\circ}13'$  east longitude and  $29^{\circ}66'$  north latitude were filled in. The outdoor environment is set according to the measured parameters. However, the operating environment parameters were changed when the computational model was used to simulate the indoor thermal environment on a typical-weather day in Lhasa or Beijing. The boundary of the enclosure structure is a wall, which reflects the influence of outdoor temperature through outdoor temperature and convective heat transfer coefficient, and adopts a non-slip and standard wall function wall treatment method. The detailed thermal properties of the building's structure are displayed in Table 2 and the parameters of the windows are shown in Table 4. According to the results of the field survey, the influence of

curtains is ignored when calculating the heat transfer process of the outer window. The boundary condition of the indoor heat source is block; the heat dissipation and temperature are shown in Table 3.

**Table 4.** Parameters of glass window.

Parameters	Values
Density	2500 (kg/m <sup>3</sup> )
Specific heat capacity	700 (J/kg·K)
Emissivity	0.84
Solar absorption rate-normal incidence	0.14
Solar transmittance-normal incidence	0.78
Solar reflectance-normal incidence	0.08

### 3. Results

#### 3.1. Measured Data and Analysis

According to the measured data of the office room, the outdoor air temperature in Lhasa ranged between 0.05 °C and 17.96 °C, and the indoor air temperature between 17.01 °C and 24.05 °C. It is indicated in Figure 7 that, similar to the outdoor air temperature, the indoor air temperature rose from morning to afternoon and fell at about 5 p.m., but the daily range of the outdoor air temperature was much greater than that of the indoor temperature. This is mainly due to the thermal inertia of the building, the use of radiators, and the fact that the windows and door were kept almost closed. Moreover, the average indoor air relative humidity stayed stable, around 21%, while the outdoor air relative humidity fluctuated between 6.11% to 77.21%.

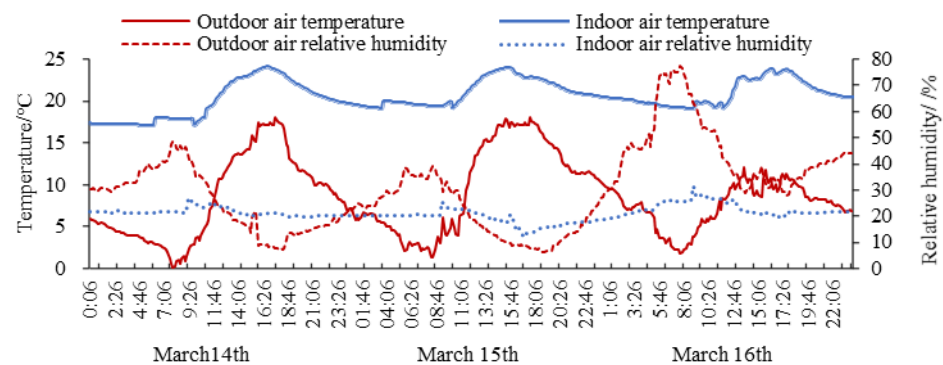


**Figure 7.** Outdoor and indoor air temperature and relative humidity.

The variations in the average internal wall temperatures at different locations during the three days are shown in Figure 8. The wall temperature generally increased with the height, and the largest wall temperature difference among the locations from 50 cm to 200 cm was 2.6 °C. The average internal wall temperatures of the east wall, west wall, and north wall were 15.53 °C, 14.6 °C and 14.5 °C, respectively. However, the temperature of the window was not measured. The wall temperature difference could be a hint of indoor air stratification.

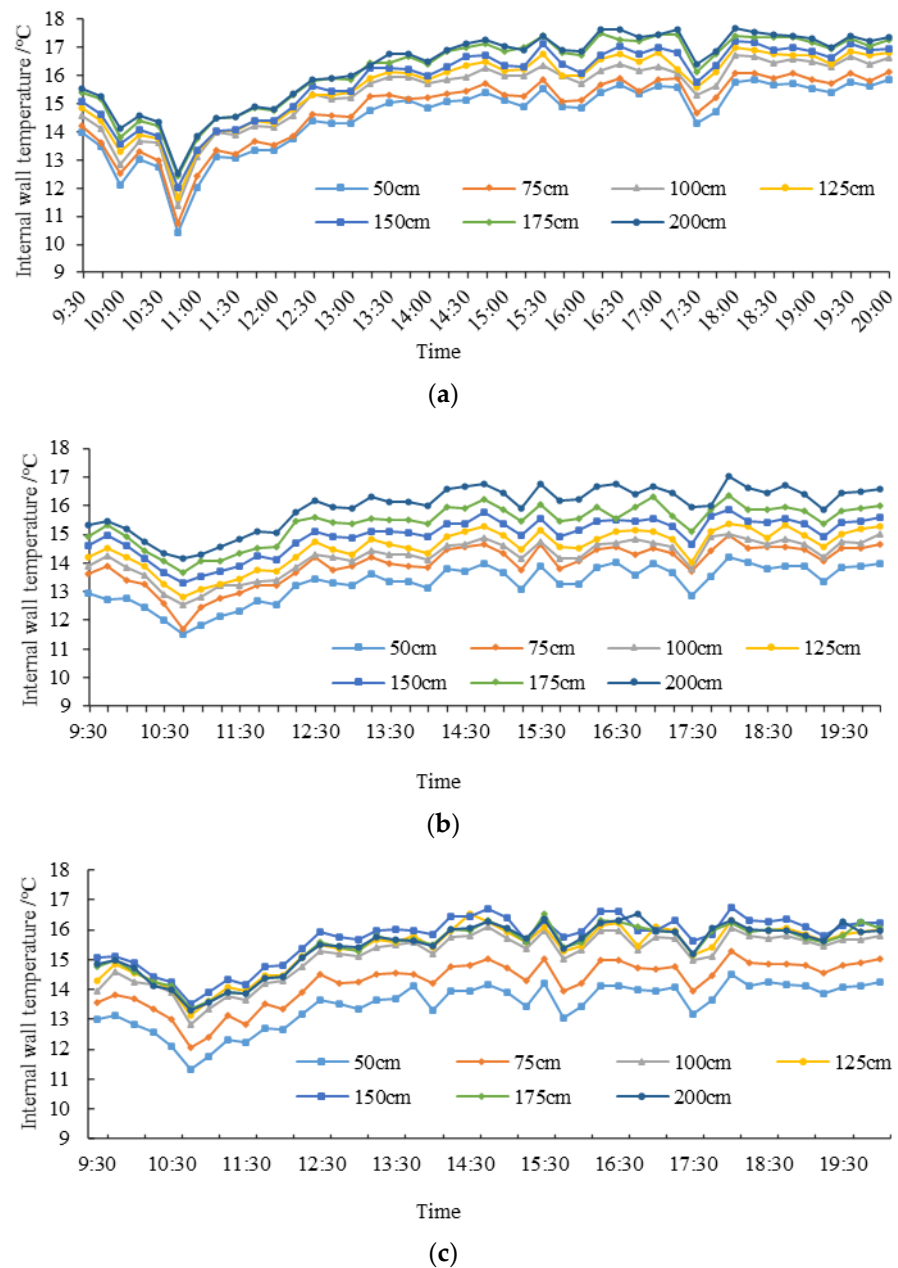


**Figure 8.** Variations in wall temperature at different locations with time: (a) east wall; (b) west wall; (c) north wall.

### 3.2. Model Verification

To examine the accuracy of the computational model, the results from 14 March were compared. The input ambient environment parameters are the measured data. The solar load model parameters include local time and position. The sunshine fraction and ground reflectance were 1 and 0.2, respectively. Figure 9 presents the relative errors of air temperature on the test point between the simulation and the experiment at different times. The measured air temperatures at 11:30, 14:30, and 17:30 were 19.32 °C, 22.79 °C, and 23.67 °C, respectively. The simulated results agreed well with the measured data. The calculated relative errors were within 2%. The west wall temperatures are shown in Figure 10; the simulated and measured wall temperatures had the same change trend, with the height rising from 50 cm to 200 cm. The simulated wall temperature was higher than that of the measured temperature by 2.62 °C. This was because the thermal inertia of the envelope was not considered in the simulation. The actual ground temperature was lower,

and the measured temperature stratification was more obvious. Nevertheless, the relative error of the wall temperature at different times was less than 15%. These results illustrate that the developed CFD model can reflect the indoor temperature with sufficient accuracy.

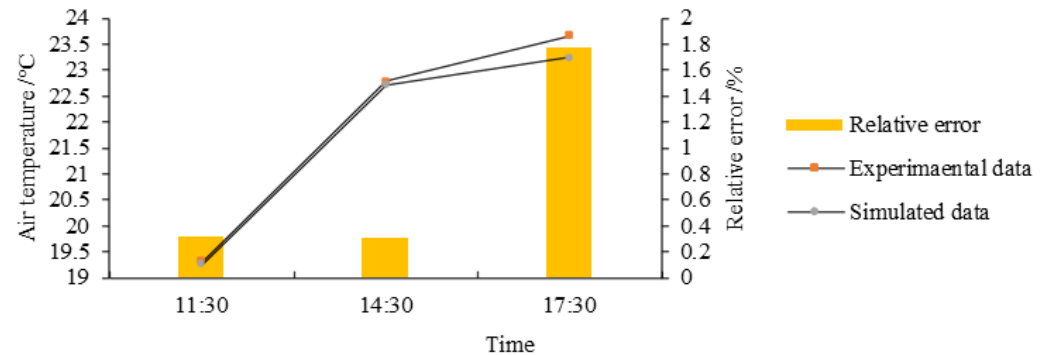


**Figure 9.** Comparisons of measured and simulated indoor air temperature.

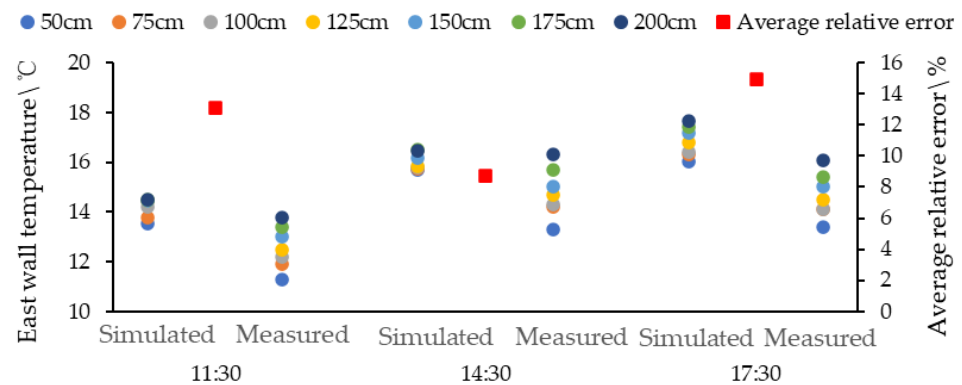


**Figure 10.** Comparisons of measured and simulated west wall temperature.

### 3.3. Simulation Results

The simulated air temperature distribution at 2:30 pm on 14 March is shown in Figure 11. The horizontal temperature field at the height of 0.6 m is not evenly distributed. On the one hand, the air temperature was affected by heat sources, resulting in higher air temperature near the heat source areas. On the other hand, with the heat fluxes from solar radiation and radiators, the indoor air temperature in the southern area was higher than in the northern area. According to the simulation results, the air temperature had obvious stratification in the vertical direction, and the temperature rises with the increase in height, which had the same trend as the internal wall temperature. In addition, the temperature of the south-facing window was much higher than that of the north-facing window.

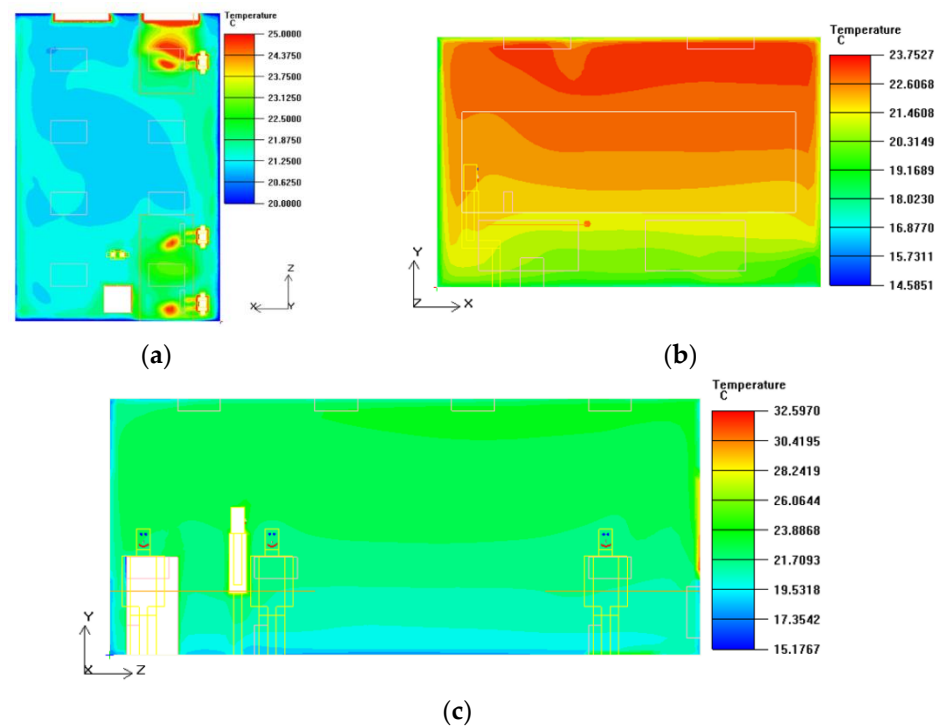


**Figure 11.** Air temperature distribution at 2:30 pm on 14 March: (a)  $Y = 0.6$  m; (b)  $Z = 3.45$  m; (c)  $X = 2.3$  m.

#### 4. Discussion

Beijing and Lhasa are both located in cold areas, with an altitude of 43.5 m and geographic coordinates of  $116^{\circ}25'$  east longitude and  $39^{\circ}54'$  north latitude. A comparison between these two cities can easily explain the difference in indoor thermal environment between the plateau and plain cold areas. Since the model was verified by the measured data in Section 3, it can be used to conduct a more in-depth analysis of the indoor thermal environment in Lhasa and Beijing. For example: What is the indoor thermal environment on a typical day in winter? It can be seen from the results of the measured and simulated temperatures that the vertical and horizontal indoor temperature differences are relatively large. Therefore, this section mainly analyzes the non-uniform distribution of indoor temperature comparatively.

##### 4.1. Typical-Weather Day in Lhasa and Beijing

The meteorological parameters of typical weather days in Lhasa and Beijing in January are shown in Figure 12 [36]. As can be seen from Figure 12a, the outdoor air temperature is below  $0^{\circ}\text{C}$  in the forenoon in the two cities. Furthermore, the temperature in Lhasa ranges from  $-7.6^{\circ}\text{C}$  to  $5.8^{\circ}\text{C}$ , with a diurnal range of  $13.4^{\circ}\text{C}$ , but the temperature in Beijing varies from  $-6.6^{\circ}\text{C}$  to  $1.2^{\circ}\text{C}$  with a diurnal range of  $7.6^{\circ}\text{C}$ . The time zone in Lhasa is two hours later than that in Beijing. Thus, the solar radiation intensity in Lhasa is two hours behind the actual values in Figure 12b. This is almost identical to Beijing, but Lhasa's direct solar radiation intensity is significantly higher than that of Beijing. As a result, the global solar radiation intensity in Lhasa is higher. At midday, the global solar radiation intensity in Lhasa is  $696\text{ W/m}^2$ , but in Beijing it is  $411\text{ W/m}^2$ . Consequently, the outdoor temperature in Lhasa exceeds that of Beijing in the afternoon, resulting in a higher daily average temperature in Lhasa. Due to the time difference, the highest measured temperatures in Lhasa and Beijing occurred at 17:00 and 15:00, respectively.

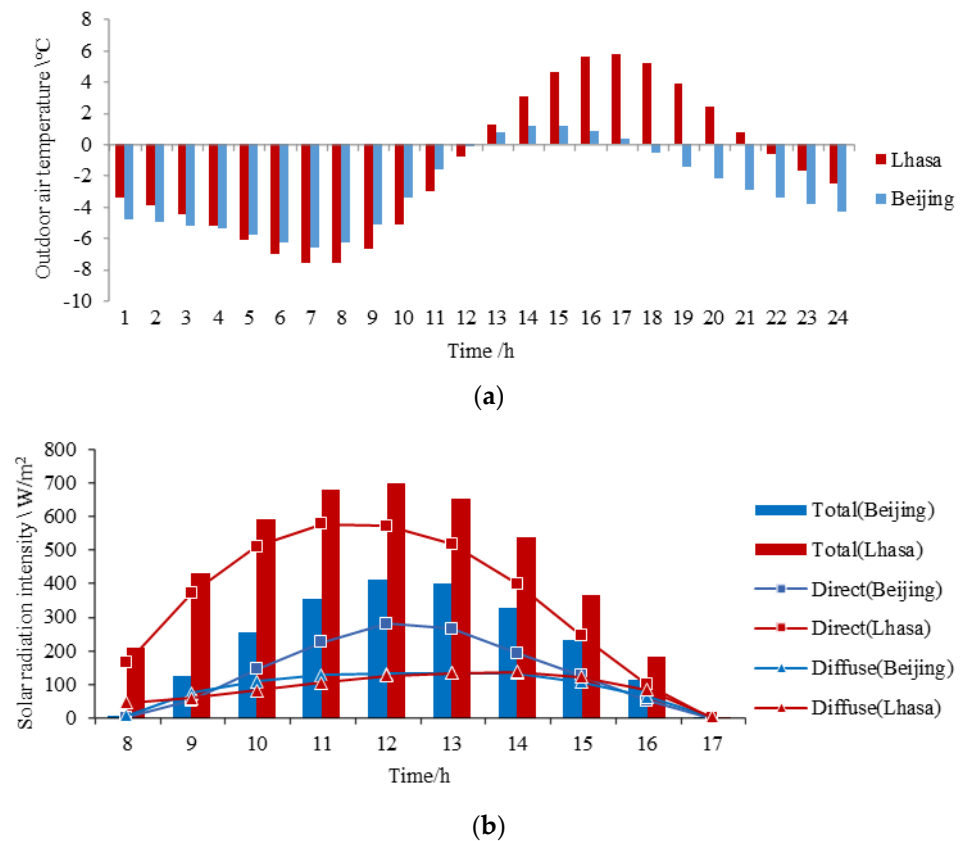


**Figure 12.** The typical weather day: (a) hourly outdoor air temperature; (b) hourly solar radiation intensity.

#### 4.2. Human Exposure Positions

The RTA value depends on the view factor between the human body and the surrounding surface. Different parts of the human body, the surfaces of the building envelope, and the heat source will produce different net radiative heat transfers, resulting in inconsistent radiant temperatures of various parts of the human body surface. The difference between the radiation temperature of the plane of the two opposite sides for the human body is RTA. Hence, six indoor points were selected as the human body position to study the non-uniform thermal distribution under the influence of a unique climate, as shown in Figure 13. In this model, the seated persons are facing east (X-axis reverse). The numerical model settings of the building envelope, radiator, and lamps are consistent with Section 2.2.

#### 4.3. Average Temperature

Figure 14 shows the variation in the average air temperature and radiation temperature on a horizontal surface at a height of 0.6 m. The indoor air temperature and radiation temperature have the same changing trend, and the difference between the two is small. Corresponding to the change in outdoor air temperature, in the morning, the air temperature in Beijing is higher, and a greater daily air temperature difference is evident in Lhasa. However, the maximum air temperature in the two cities does not exceed 15 °C, which is lower than the requirements of the “Design Standard for Heating and Ventilation of Civil Buildings for Tibet” (DBJ 540002-2016) [37] and the “Design Code for Heating Ventilation and Air Conditioning of Civil Buildings” (GB 50736-2012) [26], which are 18–24 °C. Moreover, the indoor air temperature is also lower than the neutral temperature that is proposed in existing research conclusions [10,12,13]. This shows that the current heating plan cannot make rooms reach a comfortable state. Even in March, indoor personnel still need to wear down jackets to keep warm in the morning. The average minimum and maximum indoor temperatures at a height of 0.6 m in Lhasa (Ta1) are 5.98 °C and 14.7 °C, respectively. It is

worth noting that the outdoor temperature in Lhasa is up to 5.7 °C higher than in Beijing, and the solar radiation is also stronger. However the indoor temperature in Lhasa is up to 4.17 °C higher than that of Beijing. Furthermore, the standard deviation (SD) of the radiation temperature is between 2.5 °C and 3 °C, and the SD of the air temperature is around 1.5 °C. In addition, the SD of the indoor air temperature at a height of 0.6 m in Beijing (Ta2) is similar to that of Ta1, but the SD of the radiation temperature at a height of 0.6 m (Tr2) is higher than that of Lhasa (Tr1) afternoon. Solar radiation has a greater impact on the radiant temperature of different indoor areas, and further analysis of non-uniform indoor radiant temperature is necessary. Therefore, the design load of central heating public buildings should match the actual situation.

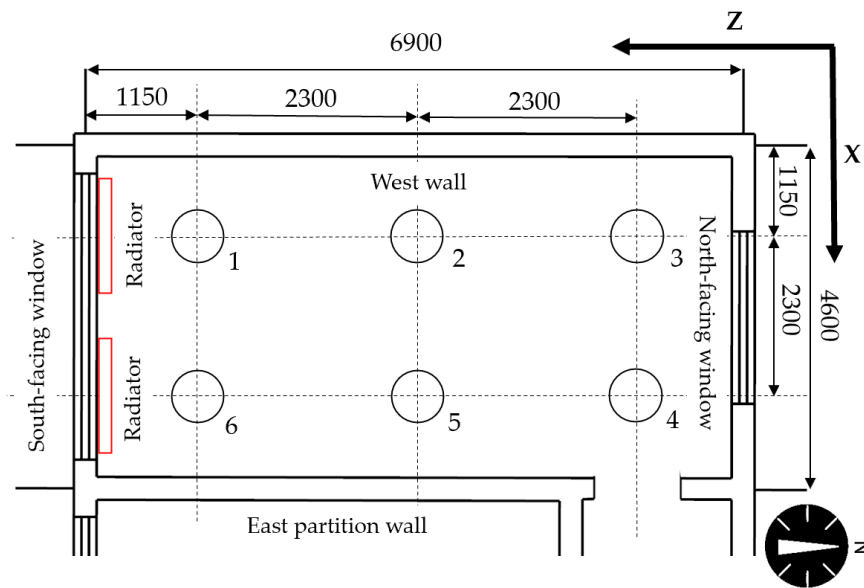


Figure 13. The human body positions in the office room.

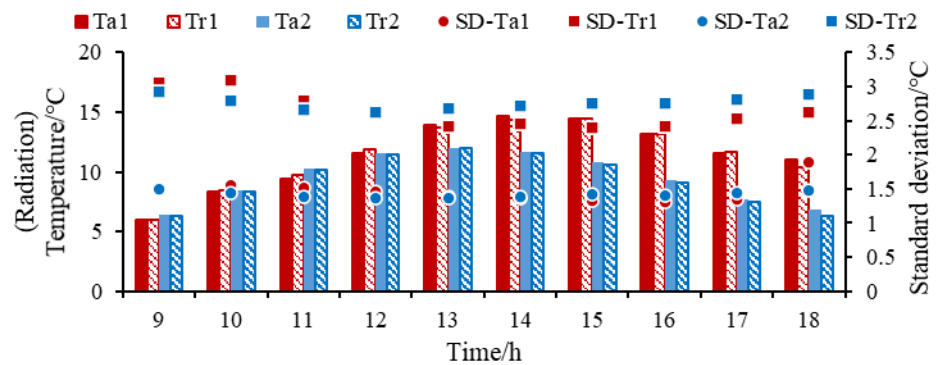


Figure 14. The average temperature and corresponding SD on a horizontal plane at the height of 0.6 m.

#### 4.4. Non-Uniform Temperature Distribution

##### 4.4.1. Vertical Air Temperature Difference

Even in the morning during March and wearing leather boots, the feet still feel uncomfortably cold. However, the body does not feel cold. In addition, as shown in Figure 11, the phenomenon of the thermal stratification of indoor air is obvious. Therefore, the VATD is a problem worth analyzing. According to the model configuration provided by the “Evaluation Standard for the Indoor Thermal Environment in Civil Buildings” (GB/T 50785-2012) [38] and ISO 7730-2005 [23], when the human body is in a sitting position, the air temperature around the head and ankles are set to 1.1 m and 0.1 m, respectively. In addition, the percentage of dissatisfaction  $LPD_2$  caused by the VATD is calculated according to [23,38]:

$$LPD_2 = \frac{100}{1 + \exp(5.76 - 0.865 \times \Delta t_{a,v})} \quad (10)$$

where  $\Delta t_{a,v}$  is the VATD between head and ankle, °C. ISO 7730-2005 stipulates that the above formula should only be used  $\Delta t_{a,v} < 8$  °C [23].

According to the simulation results, the air temperature around the ankle and head of the human body at different positions is similar to the changing trend in indoor temperature at a height of 0.6 m. Lhasa has a wider range of temperature changes, and the air temperature at various locations in the morning is lower than in Beijing. Since the outdoor temperature of Lhasa and Beijing in the morning is below 0 °C, the indoor temperature is very low, even near the radiator (position 1 (P1) and position 6 (P6)). When the solar radiation and outdoor temperature are low, the building exterior envelopes are in a heat-loss state. The temperature in different positions is low, and the temperature difference is small. Because this area is far away from the radiators, the air temperature around the ankle in position 3 (P3) and position 4 (P4) is lower than in other positions. The lowest temperatures near the ankle in Lhasa and Beijing are 3.71 °C and 4.33 °C, respectively. When the solar radiation is strong, the indoor temperature is relatively high. The temperature around the head in position 2 (P2) can reach 15.8 °C. The temperature difference between different positions in the room is obvious. This is because part of the indoor area receives heat from solar energy. In addition, the south outer wall (window) is in a state of heat gain, while the north outer wall (window) is still in a state of heat loss.

Figure 15a calculates the VATDs between the ankle and the head, and Figure 15b lists the corresponding  $LPD_2$ . The vertical temperature difference between Lhasa and Beijing is less than 3 °C most of the time, and the  $LPD_2$  is also within 5%. Generally, P3 has the largest vertical temperature difference due to its proximity to the west and north outer wall. The maximum vertical temperature differences between Lhasa and Beijing are 3.12 °C and 3.2 °C, and the corresponding dissatisfaction rates are 4.87% and 5.21% (in Figure 15b). According to the requirements of ISO 773-2005 [23], the VATD should be less than 3 °C (category B) or 4 °C (category C), and the corresponding  $LPD_2$  is 10%. Moreover, the strictest limit for  $LPD_2$  is 10% in GB/T 50785-2012 [38]. Therefore, the indoor vertical temperature difference in Lhasa and Beijing meets the requirements of ISO 773-2005 and GB/T50785-2012. However, ASHRAE 55-2017 [27] stipulates that  $LPD_2$  should be less than 5%.

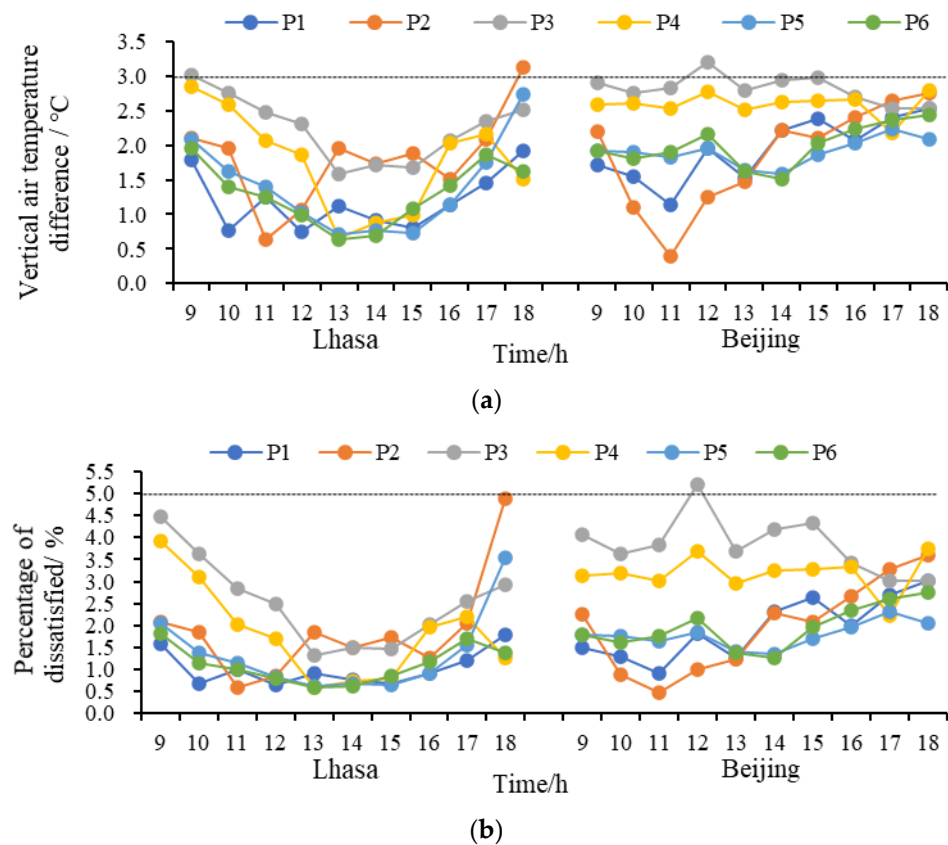


**Figure 15.** Diurnal variations of VATD: (a) vertical temperature differences; (b) percentage of dissatisfied.

#### 4.4.2. Radiant Temperature Asymmetry

According to the concept of RTA proposed by Fanger [18,19], human RTA can be evaluated in three orthogonal directions: chest and back (X-axis), head and ankles (Y-axis), and left and right arms (Z-axis). Equation (11) can calculate the dissatisfaction rate caused by asymmetric radiation due to cold walls (windows). However, this equation is only applicable to the asymmetry of the left and right arms [23].

$$LPD_4 = \frac{100}{1 + \exp(9.93 - 0.5 \times \Delta t_{pr})}, \Delta t_{pr} < 15 \text{ } ^\circ\text{C} \quad (11)$$

where  $LPD_4$  is the percentage of dissatisfied people due to radiant asymmetry, %.  $\Delta t_{pr}$  is RTA,  $^\circ\text{C}$ .

The RTA of the human body in different directions is shown in Figure 16. In general, the radiant asymmetry in Lhasa is more obvious than in Beijing. The RTA in the X direction is the average radiant temperature difference between the chest and the back. A negative value indicates that the back temperature of the human body is higher. As shown in Figure 16a, the RTA of indoor position 5 (P5) in the two cities is the largest. The RTA in Lhasa ranges from 1.1  $^\circ\text{C}$  to 2.53  $^\circ\text{C}$  and the RTA in Beijing ranges from 1.6  $^\circ\text{C}$  to 2.8  $^\circ\text{C}$ . In addition, the radiation temperature of the back at P6 is higher than that of the chest. The RTA value of Lhasa in this position is greater, with a maximum value of  $-1.6 \text{ } ^\circ\text{C}$ . On the one hand, the back receives more heat radiation from the radiators. On the other hand, the back receives solar energy. The RTA value of the third position in Beijing is similar to that of Lhasa, but after 16:00, the radiation temperature of the chest is lower than that of the back. It may be that the outdoor temperature drops, causing the cold radiation of the north outer window to be stronger than that of the west outer wall. The RTA value in other positions is positive because the person is facing the east inner wall and their back is facing the west outer wall.

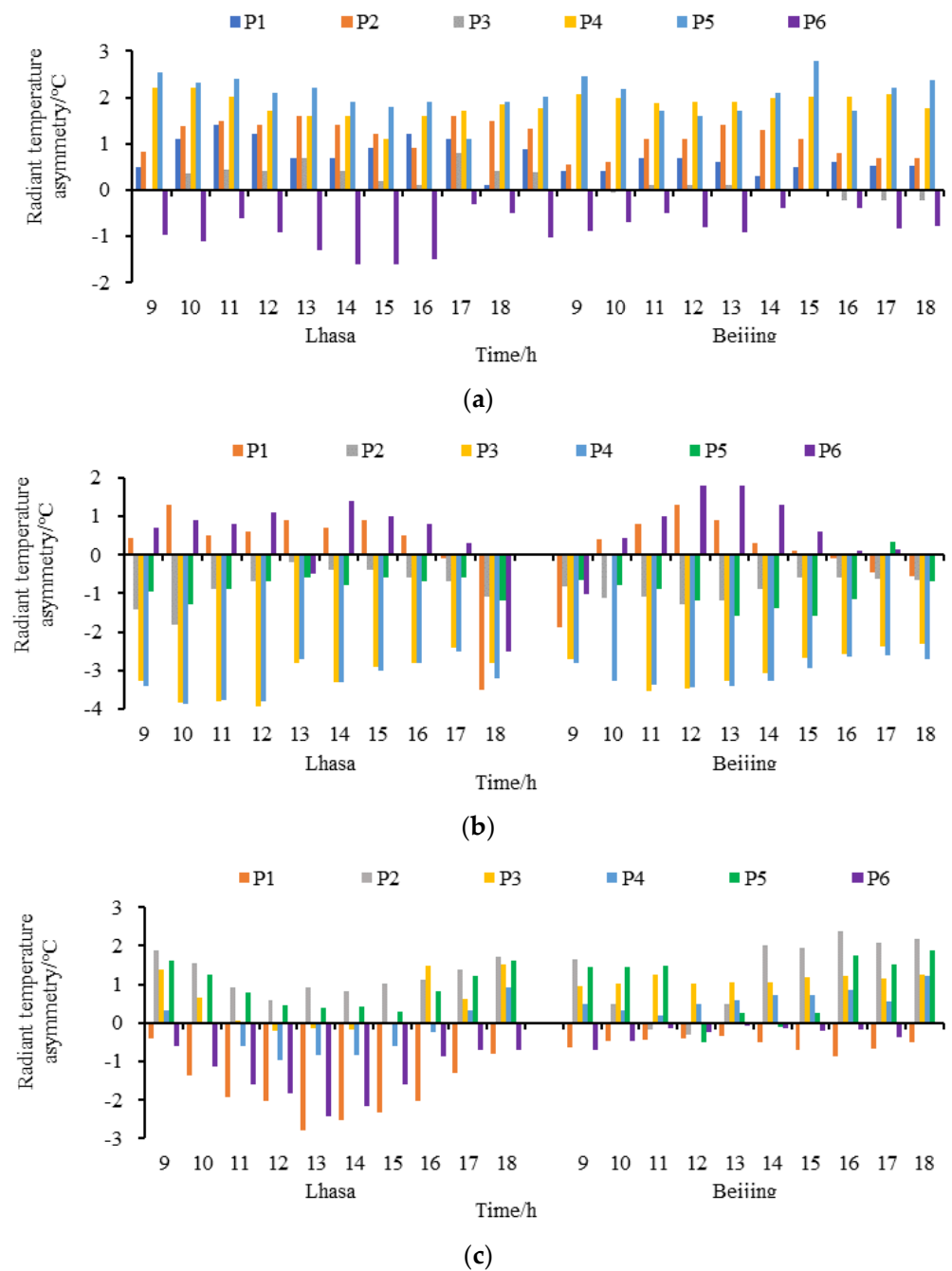


**Figure 16.** Diurnal variations of RTA in different directions: (a) chest and back (X-axis); (b) left and right arms (Z-axis); (c) head and ankle (Y-axis).

The RTA in the Z direction refers to the average radiation difference between the left arm and the right arm. The distribution trend in RTA at different positions in Lhasa and Beijing is the same most of the time, but there is a big difference at 9:00 and 18:00, as shown in Figure 16b. To take P1 as an example, the average radiant temperature of the left arm in Lhasa is higher than that of the right arm at 9:00, while the temperature of the right arm is higher in Beijing. At this juncture, the solar radiation intensity in Lhasa is  $0 \text{ W/m}^2$ , and the outdoor air temperature is as low as  $-6.7 \text{ }^\circ\text{C}$ . The south outward window is the heat loss surface, which can be regarded as a cold radiant panel. The human body receives more cold radiation from the external window than heat radiation from the radiator. However, the total solar radiation intensity at 9:00 in Beijing is  $125 \text{ W/m}^2$  and the outdoor air temperature is  $-5.1 \text{ }^\circ\text{C}$ . The right arm of the human body in P1 receives more

heat than the left arm. At 18:00, the RTA of Lhasa and Beijing at location 1 are  $-3.5\text{ }^{\circ}\text{C}$  and  $-0.57\text{ }^{\circ}\text{C}$ , respectively. In addition, the average radiation temperature of the right arm in Beijing is higher after 16:00. This is because the sunrise and sunset times are different, since they are affected by the time difference between the two cities. Overall, the RTA in the Z direction of Lhasa is higher, reaching  $-3.95\text{ }^{\circ}\text{C}$ , with an  $LPD_4$  of 0.52% at P4.

The RTA in the Y direction refers to the average radiant temperature difference between the head and ankle, as shown in Figure 16c. The ankle receives more heat than the head when the human body is seated in P1 and P6. Therefore, the radiation temperature of the ankle is higher than that of the head, resulting in a negative RTA in the Y direction. Lhasa has the largest RTA at P1 in the Y direction, which can reach  $-2.79\text{ }^{\circ}\text{C}$ , with an  $LPD_4$  of 0.35%. The RTA of Beijing at P1 is relatively small, with a maximum of  $-1.86\text{ }^{\circ}\text{C}$ . When individuals are in P2 and P5, they are far away from the outer window and receive less cold radiation. Therefore, the average radiant temperature of the head is relatively high, and the RTA in Lhasa is positive in the Y direction. In addition, the average radiant temperature of the head in P4 in Lhasa is lower than that of the ankle when the solar radiation is strong. This can be explained by the fact that the radiation temperature on the side of the head near the radiators and the south outer window is higher, and the radiation temperature on the other sides is lower, especially the left side near the north outer window. Nevertheless, the ankle is far from the outer window, and its average radiation temperature is relatively high. Due to the relatively weak solar radiation in Beijing, the influence of solar energy on indoor radiant temperature is small. Coupled with the influence of outdoor temperature, the average radiant temperature of P4 in Beijing is lower than that in Lhasa. At noon, the average radiant temperature of the head and ankle of P4 in Lhasa are  $12.6\text{ }^{\circ}\text{C}$  and  $13.56\text{ }^{\circ}\text{C}$ , while the average radiant temperatures of Beijing at that this position are  $12.2\text{ }^{\circ}\text{C}$  and  $11.96\text{ }^{\circ}\text{C}$ , respectively. The cold radiation caused by the north outer window on the head has a weaker effect on the average radiation temperature than the indoor thermal stratification. Therefore, the RTA of Beijing P4 in the Y direction is positive.

Taking the simulation result at 10:00 in Lhasa as an example, it is possible to further analyze the human body radiation temperature at indoor location 4. Figure 17 is the radiation temperature cloud diagram of the front chest and back at indoor location 4 in Lhasa. At this time, the average radiation temperatures of the human chest and back are  $9.54\text{ }^{\circ}\text{C}$  and  $7.32\text{ }^{\circ}\text{C}$ , respectively. Affected by the cold radiation from the north outer window, the radiation temperature of the central axis of the chest and back increases with the decrease in height. In addition, the radiant temperature on the left side of the human body (near the north outer window) is much lower than on the right side, as is clearly manifested by the head, arms, back, and legs. Figure 14 is also a cloud map of the radiation temperature on the left and right sides of the human body at P4 in Lhasa. The difference in radiation temperature between the left and right arms of the human body is more evident. The average radiation temperature of the left arm and right arm are  $5.94\text{ }^{\circ}\text{C}$  and  $9.8\text{ }^{\circ}\text{C}$ , respectively. The radiant temperature of the head and ankles on the same side is little different. However, the low temperature of the north outer window causes the temperature on the left side of the head to be significantly lower than that on the right side, and the maximum radiant temperature difference reaches  $8.73\text{ }^{\circ}\text{C}$ , with an  $LPD_4$  of 2.66%.

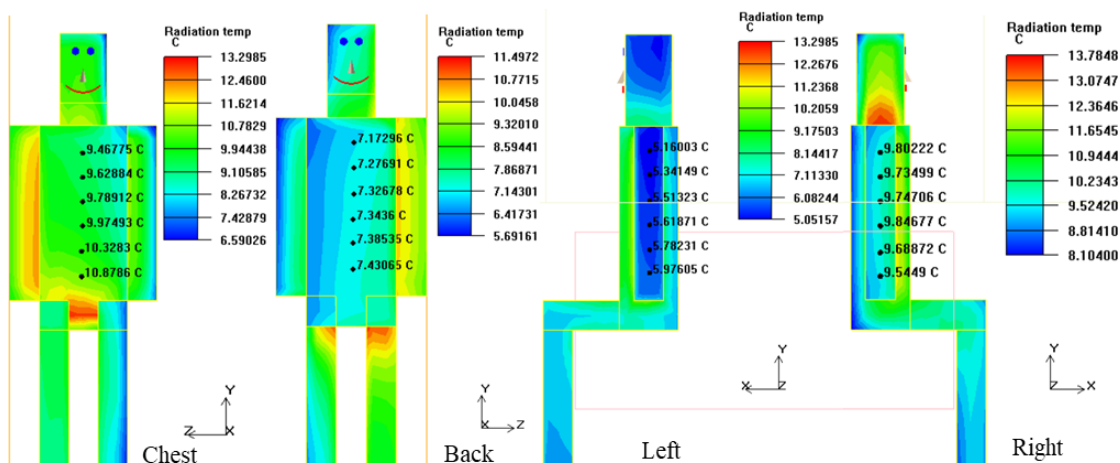


**Figure 17.** Radiation temperature for the human body in point 4 of Lhasa at 10:00.

In summary, there are certain differences in the indoor thermal environment between Lhasa and Beijing. Under the same envelope structure and heating conditions, the average indoor temperature and average radiant temperature in Lhasa are higher, and the non-uniform of indoor temperature distribution in Lhasa is also more significant. The indoor temperature in both cities is below comfortable levels. The indoor vertical temperature difference between Lhasa and Beijing meets the requirements of ISO 7730-2005 [23] and GB/T50785-2012 [38]. In general, the indoor RTA in Lhasa is larger than in Beijing and lower than the limits set by the current standard. The RTA in the Z direction is the largest. This is due to the large heat loss of the north outer window on the left side of the human body, while the right side can obtain the heat from the radiator and the solar energy passing through the south outer window. Lhasa's position near the north outer window received strong cold radiation, resulting in higher RTA during certain periods. This shows that direct solar radiation through windows helps to improve thermal comfort. Due to thermal stratification, the air temperature at the height of 1.1 m in Lhasa and Beijing is higher than at 0.1 m. The average radiant temperature of the head in indoor P1 and P6 is lower than the average radiant temperature of the ankle. In addition, the average radiation temperature of the head in P4 is lower than that of the ankle during periods of strong solar radiation in Lhasa. This shows that the cold radiation from outer windows in the cold plateau area has a greater impact on the indoor thermal environments to which human bodies are subjected, even when the temperature is high during the day.

#### 4.5. Analysis of Standards

At present, there are two standards for the design and evaluation of indoor thermal environment in Tibet. The regulations on the lighting, ventilation, heat preservation, and heat insulation of building layouts, orientations, and forms can be found in the "Design Standard for Green Building in the Tibet Autonomous Region" (DBJ540001-2018) [39]. Moreover, the standard also requires that indoor thermal comfort should consider dry bulb temperature, air humidity, airflow speed, average radiant temperature difference, and indoor personnel activities and clothing conditions. However, there is no clear description of the concept, calculation method, and limit of the average radiant temperature difference. The "Design Standard for Heating and Ventilation of Civil Buildings for Tibet" (DBJ540002-2016) stipulates that the main room should be 18–24 °C and that the wind speed of the heating indoor activity area should be lower than 0.3 m/s [37]. The national indoor thermal environment design and evaluation standards include GB 50736-2012 and GB/T 50785-2012. In GB 50736-2012, the indoor thermal environment with a temperature of 18–22 °C, relative humidity of more than 30%, and wind speed of less than 0.2 m/s is classified as level I. When the indoor temperature is 22–24 °C and the wind speed is lower than 0.2 m/s, which can be considered as meeting level II [26]. The evaluation of the overall indoor thermal

environment for GB/T 50785-2012 is consistent with GB 50736-2012. Furthermore, the grades and limits of local thermal comfort are supplemented in GB/T 50785-2012, but the impact of radiant asymmetry on local comfort is not included [38]. ISO 7730-2005 and ASHRAE 55-2017 present comprehensive and detailed regulations on local thermal comfort. The limits of the vertical temperature difference and RTA of category A for ISO 7730-2005 are 2 °C and 10 °C (cool wall), and the corresponding percentages of dissatisfied people are 3% and 5%, respectively [23]. In addition, the upper limits of ASHRAE standard 55-2017 for vertical temperature difference (sitting posture) and RTA (cool wall) are 3 °C and 14 °C, respectively, and the corresponding dissatisfaction rate is 5%. However, the RTA limits of the ASHRAE 55 standard are applicable when the ambient temperature is within thermal comfort levels for a lightly clothed person engaged in near-sedentary physical activity. In addition, they may underestimate local discomfort when the temperature is lower than comfortable levels. However, the results presented by Su et al. show that the RTA limit under radiator heating is 1.6 °C [40].

It can be seen that corresponding indoor thermal environment standards in cold plateau areas help to guide the design of buildings and indoor thermal environment parameters. However, the guidance for the design of indoor thermal parameters in the unique climate of the alpine region is not perfect. The indoor thermal parameters are limited, but their particularity is not considered. The non-uniform distribution of indoor temperatures in the cold plateau regions is caused by low outdoor temperatures, strong solar radiation, and heating. However, the local thermal discomfort caused by non-uniform indoor temperatures is not mentioned in the local standards. Moreover, when the indoor temperature is low, the local discomfort of the human body is more sensitive. Although detailed regulations on non-uniform indoor local thermal comfort can be found in ISO 7730 and ASHRAE 55, the limits are set according to certain indoor conditions and the relative position between the human body and the environment. They do not apply to the evaluation of indoor local thermal comfort in Tibetan Plateau areas.

## 5. Conclusions

A unique indoor thermal environment is created by the climatic characteristics of the Tibetan Plateau, but a comprehensive understanding of the indoor thermal environment cannot be found in relevant research. In this study, the non-uniform distribution of radiant temperature was evaluated and analyzed comparatively. In short, the following conclusions can be drawn:

(1) According to the field measurement results in March, the selected office room stayed within the comfortable temperature range. Furthermore, the temperature of the inner wall increased with the height of the location due to thermal stratification.

(2) On a typical-weather day in the winter in Lhasa and Beijing, the maximum indoor average temperature at the height of 0.6 m is 14.7 °C. The VATD of Lhasa and Beijing are below 3 °C most of the time. However, the asymmetry of the indoor radiant temperature in Lhasa is more notable. The maximum RTA of the human body and the head, respectively, are −3.95 °C and 8.73 °C.

(3) Due to the strong solar radiation and low temperature in the Tibetan Plateau, indoor thermal comfort is greatly affected by the ambient environment. Architectural designs should try to avoid setting north-facing windows in this area to reduce heat loss.

(4) A comprehensive standard should be compiled based on the characteristics of non-uniform indoor thermal environments in cold plateau areas for building thermal environment definition, calculation, design, and evaluation.

Moreover, future developments of this research may include:

(1) A study of the indoor thermal environment characteristics of residential buildings. It is severely cold, particularly in winter, in the Tibetan Plateau.

(2) A subjective questionnaire survey of overall thermal sensation and local thermal sensation at the same time as environmental measurements including air temperature, air relative humidity, air speed, and radiant temperature.

(3) An investigation of the indoor thermal environment in other seasons and the impact of the results on the design of buildings.

**Author Contributions:** Conceptualization, M.W. and P.S.; methodology, M.W.; software, M.W.; validation, M.W.; formal analysis, P.S.; investigation, M.W.; resources, P.S.; data curation, M.W.; writing—original draft preparation, M.W.; writing—review and editing, P.S.; visualization, M.W.; supervision, P.S.; project administration, P.S.; funding acquisition, P.S. All authors have read and agreed to the published version of the manuscript.

**Funding:** This research was funded by “National Natural Science Foundation of China (NSFC), grant number 52008132”, “Basic and Applied Basic Research Foundation of Guangdong Province, China, grant number. 2019A1515111194”, and “Shenzhen Science and Technology Program, grant number. RCBS20200714114921062”.

**Institutional Review Board Statement:** Not applicable.

**Informed Consent Statement:** Not applicable.

**Data Availability Statement:** The study did not report any data.

**Conflicts of Interest:** The authors declare no conflict of interest.

## Nomenclature

$a$	Absorption coefficient	$\vec{s}$	Scattered direction
$C_p$	Specific heat of air, J/(kg·K)	$T$	Air temperature, °C
$g_i$	Gravitational acceleration vector, m/s <sup>2</sup>	$Ta1$	Average indoor air temperature at the height of 0.6 m of Lhasa, °C
$I$	Radiation intensity depending on location ( $\vec{r}$ ) and direction ( $\vec{s}$ ), w/m <sup>2</sup>	$Ta2$	Average indoor air temperature at the height of 0.6 m of Beijing, °C
$l$	Nearest distance from the wall, m	$T_c$	Reference air temperature, °C
$LPD_2$	Percentage of dissatisfaction caused by vertical air temperature difference, %	$Tr1$	Average indoor radiation temperature at the height of 0.6 m of Lhasa, °C
$LPD_4$	Percentage of dissatisfaction caused by radiant temperature asymmetry, %	$Tr2$	Average indoor radiation temperature at the height of 0.6 m of Beijing, °C
$n$	Convert coefficient	$u$	Tangential velocity of the wall, m/s
$P$	Partial pressure of water vapor in moist air, Pa	$u_i$	Air velocity component in point $x_i$ , m/s
$Pr_t$	Turbulent Prandtl number	$u_j$	Air velocity component in point $x_j$ , m/s
$\vec{r}$	Position vector	$u_\tau$	Friction velocity of wall, m/s
$s$	Length path, m	$y$	Normal distance from wall to first layer of mesh, m
$\vec{s}$	Directional vector		
<i>Greek symbols</i>			
$\alpha$	Coefficient of cubical expansion	$\rho$	Air density, kg/m <sup>3</sup>
$\beta$	Thermal expansion coefficient, K <sup>-1</sup>	$\rho_c$	Air density corresponding $T_c$ , kg/m <sup>3</sup>
$\lambda_{eff}$	Effective thermal conductivity, W/m·°C	$\rho_w$	Density of wall, kg/m <sup>3</sup>
$\lambda_l$	Laminar effective thermal conductivity, W/m·°C	$\sigma$	Stefan–Boltzmann constant, $5.672 \times 10^{-8}$ W/m <sup>2</sup> k <sup>4</sup>
$\mu$	Dynamic viscosity, (N·s)/m <sup>2</sup>	$\sigma_s$	Scattering coefficient
$\mu_{eff}$	Effective viscosity, Pa·s	$\Delta t_{a,v}$	Vertical air temperature difference between head and ankle, °C
$\mu_l$	Laminar viscosity, Pa·s	$\Phi$	Phase function
$\mu_t$	Turbulent viscosity, Pa·s	$\Omega'$	Spatial angle
$v$	Local mean velocity, m/s		
<i>Abbreviations</i>			
ASHRAE	American society of heating, refrigerating and air-conditioning engineers	ISO	International Standards Organization
CFD	Computational fluid dynamics	SD	Standard deviation
RTA	Radiant temperature asymmetry	VATD	vertical air temperature difference

## References

1. Tibet Plateau. Available online: <https://baike.baidu.com/item/%E8%A5%BF%E8%97%8F%E9%AB%98%E5%8E%9F/9701346?fr=aladdin> (accessed on 25 December 2021). (In Chinese).
2. Overview of Land Resources in Tibet Autonomous Region. Available online: [http://www.xizang.gov.cn/rsxz/qj/zrdl/201812/t20181221\\_34484.html](http://www.xizang.gov.cn/rsxz/qj/zrdl/201812/t20181221_34484.html) (accessed on 21 December 2018).
3. The 2018 Statistical Communique on National Economic and Social Development of the Tibet Autonomous Region. Available online: [http://www.xzwx.com/xw/xzyw/201905/t20190528\\_2635687.html](http://www.xzwx.com/xw/xzyw/201905/t20190528_2635687.html) (accessed on 18 May 2019).
4. Wang, D.J.; Liu, Y.F.; Wang, Y.; Liu, J.P. Measurement and Evaluation of Indoor Thermal Environment of Residential Buildings in Lhasa in Winter. *Build. Sci.* **2011**, *27*, 20–24. [CrossRef]
5. Li, E.; Zhu, J.K. Parametric analysis of the mechanism of creating indoor thermal environment in traditional houses in Lhasa. *Build. Environ.* **2021**, *207*, 108510. [CrossRef]
6. Qi, F.; Yang, L.; He, Q.; Liu, D.; He, H.; Wang, Q.Q. Residential Indoor Thermal Environment Test and Analysis of Kangding in Winter. *Build. Energy Effic.* **2015**, *3*, 102–106. [CrossRef]
7. Wang, P.Q.; Leng, Y.H.; Xu, G.T. Analysis on Thermal Environment Current Situation of Residential Buildings in the South-Eastern of Tibet. *Build. Sci.* **2012**, *28*, 65–68. [CrossRef]
8. Sun, H.J.; Leng, M.J. Analysis on building energy performance of Tibetan traditional dwelling in cold rural area of Gannan. *Energy Build.* **2015**, *96*, 251–260. [CrossRef]
9. Wang, Z. Passive Design of Energy Efficient Residential Building in Chamdo. Master's Thesis, Xi'an University of Architectural and Technology, Xi'an, China, 2014.
10. Zhang, M. The Passive Control Strategy Research of Residential Buildings Indoor Thermal Environment in Tibet Area. Master's Thesis, Chongqing University, Chongqing, China, 2015.
11. Xie, H. Research on Interior Thermal Environment of Architectural Design Based on High Altitudes. Master's Thesis, Southwest Jiaotong University, Chengdu, China, 2014.
12. Luo, Y. Improve the Indoor Thermal Environment of Alpine Region Building Technical Measures and Research in Tibet. Master's Thesis, Southwest Jiaotong University, Chengdu, China, 2012.
13. Yang, L.; Yan, H.Y.; Xu, Y.; Lam, J.C. Residential thermal environment in cold climates at high altitudes and building energy use implications. *Energy Build.* **2013**, *62*, 139–145. [CrossRef]
14. Zhao, J.; Lu, J.; Liao, X.; Huang, G.Q.; Li, X.L.; Guo, X.J. Influence of Solar Radiation on Indoor Thermal Environment in Cold Highland Area. *Gas Heat* **2014**, *34*, 17–21. [CrossRef]
15. Huang, L.J.; Hamza, N.; Lan, B.; Zahi, D. Climate-responsive design of traditional dwellings in the cold-arid regions of Tibet and a field investigation of indoor environments in winter. *Energy Build.* **2016**, *128*, 697–712. [CrossRef]
16. Fanger, P.O.; Bànhidi, L.; Olesen, B.W.; Langkilde, G. Comfort Limits for heated ceilings. *ASHRAE Trans.* **1980**, *86*, 141–156.
17. Fanger, P.O.; Ipsen, B.M.; Langkilde, G.; Olesen, B.W.; Christensen, N.K.; Tanabe, S. Comfort limits for asymmetric thermal radiation. *Energy Build.* **1985**, *8*, 225–236. [CrossRef]
18. Chrenko, F.A. Heated Ceilings and Comfort. *J. Inst. Heat. Vent. Eng.* **1953**, *20*, 375–396.
19. Loveday, D.L.; Parsons, K.C.; Taki, A.H.; Hodder, S.G. Displacement ventilation environments with chilled ceilings: Thermal comfort design within the context of the BS EN ISO7730 versus adaptive debate. *Energy Build.* **2002**, *34*, 573–579. [CrossRef]
20. Loveday, D.L.; Parsons, K.C.; Taki, A.H.; Hodder, S.G.; Jeal, L.D. Designing for Thermal Comfort in Combined Chilled Ceiling/Displacement Ventilation Environments. In Proceedings of the 1998 ASHRAE Winter Meeting, San Francisco, CA, USA, 17–21 June 1998; p. 1162.
21. Griffiths, I.; McIntyre, D. Subjective Response to Overhead Thermal-Radiation. *Hum. Factors* **1974**, *16*, 415–422. [CrossRef]
22. McNall, P.E.; Biddison, R.E. Thermal and comfort sensations of sedentary persons exposed to asymmetric radiant fields. *ASHRAE Trans.* **1970**, *76*, 123–136.
23. ISO 7730; Ergonomics of the Thermal Environment-Analytical Determination and Interpretation of Thermal Comfort Using Calculation of the PMV and PPD Indices and Local Thermal Comfort Criteria. International Organization for Standardization: Geneva, Switzerland, 2005; 6–10.
24. Standard 55-2004; Thermal Environmental Conditions for Human Occupancy ANSI/ASHRAE. American Society of Heating, Refrigerating and Air-Conditioning Engineers: Atlanta, GA, USA, 2004; 4–10, 26.
25. GB50178-93; National Standard of the People's Republic of China: Standard for Building Climate Zoning. China Planning Press: Beijing, China, 1994; 2–3.
26. GB 50736-2012; Design Code for Heating Ventilation and Air Conditioning of Civil Buildings. China Construction Industry Press: Beijing, China, 2012; 5–10.
27. Standard 55-2017; Thermal Environmental Conditions for Human Occupancy ANSI/ASHRAE. ASHRAE Website: Atlanta, GA, USA, 2017; 4–18. Available online: [www.ashrae.org](http://www.ashrae.org) (accessed on 12 October 2017).
28. Zhu, W.J. CFD Simulation of the Heat Environment of Multi-Spar Greenhouse at Night in Winter under Heating. Master's Thesis, China Agricultural University, Beijing, China, 2005; p. 119.
29. Echeverria Serur, C. Fast Iterative Methods for Solving the Incompressible Navier-Stokes Equations. Master's Thesis, Delft University of Technology, Delft, The Netherlands, 2013.
30. Emanuel, G. *Analytical Fluid Dynamics*; CRC Press: Boca Raton, FL, USA, 2017; p. 24.

31. Wang, F.J. *Computational Fluid Dynamics Analysis*; Tsinghua University Press: Beijing, China, 2004; pp. 7–10.
32. Chen, Q.Y.; Xu, W.R. A zero-equation turbulence model for indoor airflow simulation. *Energy Build.* **1998**, *28*, 137–144. [[CrossRef](#)]
33. Nazarian, N.; Kleissl, J. CFD simulation of an idealized urban environment: Thermal effects of geometrical characteristics and surface materials. *Urban Stud.* **2015**, *12*, 141–159. [[CrossRef](#)]
34. Guo, X.G. Study on Thermal Performance of the Heating Radiator in Cold Regions with High Altitude. Master's Thesis, Chongqing University, Chongqing, China, 2014.
35. GB/T 18048-2008; Ergonomics of the thermal environment Determination of Metabolic Rate. Administration of Quality Supervision Inspection and Quarantine of China, Standardization Administration of China, China Standard Press: Beijing, China, 2008; 11.
36. Zhang, Q.Y. *Standard Meteorological Database for Chinese Construction*; China Building Industry Press: Beijing, China, 2004; pp. 62, 138.
37. Housing and Urban-Rural Development Department of Tibet Autonomous Region. *Design Standard for Heating and Ventilation of Civil Buildings for Tibet*; Housing and Urban-Rural Development Department of Tibet Autonomous Region: Lhasa, China, 2016; p. 8.
38. GB/T50785-2012; Evaluation Standard for Indoor Thermal Environment in Civil Buildings. China Construction Industry Press: Beijing, China, 2012; 5–10.
39. DBJ540001-2018; Design Standard for Green Building in the Tibet Autonomous Region. Housing and Urban-Rural Development Department of Tibet Autonomous Region: Lhasa, China, 2018; 15–19, 37–38.
40. Su, X.W.; Wang, Z.J.; Xu, Y.Y.; Liu, N.C. Thermal comfort under asymmetric cold radiant environment at different exposure distances. *Build. Environ.* **2020**, *178*, 106961. [[CrossRef](#)]